# Accepted Manuscript


Evaluation of Vis-NIR hyperspectral imaging as a process analytical tool to classify brined pork samples and predict brining salt concentration

Achata EM, Inguglia ES, Esquerre CA, Tiwari BK, O'Donnell CP

| | |
|---|---|
| PII: | S0260-8774(18)30457-6 |
| DOI: | 10.1016/j.jfoodeng.2018.10.022 |
| Reference: | JFOE 9440 |
| To appear in: | *Journal of Food Engineering* |
| Received Date: | 24 April 2018 |
| Accepted Date: | 19 October 2018 |

Please cite this article as: Achata EM, Inguglia ES, Esquerre CA, Tiwari BK, O'Donnell CP, Evaluation of Vis-NIR hyperspectral imaging as a process analytical tool to classify brined pork samples and predict brining salt concentration, *Journal of Food Engineering* (2018), doi: 10.1016/j.jfoodeng.2018.10.022

# Evaluation of Vis-NIR hyperspectral imaging as a process analytical tool to classify brined pork samples and predict brining salt concentration

Achata EM[1], Inguglia ES[2], Esquerre CA[1], Tiwari BK[2*], O'Donnell CP[1]

[1]School of Biosystems and Food Engineering, University College Dublin, Ireland

[2]Department of Food Chemistry & Technology, Teagasc Food Research Centre, Ashtown, Dublin 15, Ireland

Address for corresponding author: Teagasc Food Research Centre, Ashtown, Dublin 15, Ireland; Email: brijesh.tiwari@teagasc.ie, Tel: 0035318059785

## Abstract

Hyperspectral imaging in the visible and near infrared spectral range (450-1664 nm) coupled with chemometrics was investigated for classification of brined and non-brined pork loins and prediction of brining salt concentration employed. Hyperspectral images of control, water immersed and brined (5, 10 or 15% salt (w/v)) raw and cooked pork loins from 16 animals were acquired. Partial least squares (PLS) discriminative analysis models were developed to classify brined pork samples and PLS regression models were developed for prediction of brining salt concentration employed. The ensemble Monte Carlo variable selection method (EMCVS) was used to improve the performance of the models developed**.** Partial least squares (PLS) discriminative analysis models developed correctly classified brined and non-brined samples, the best classification model for raw samples (Sen = 100%, Spec = 100%, G = 1.00) used the 957–1664 nm spectral range, and the best classification model for cooked samples (Sen = 100%, Spec = 100%, G = 1.00) used the 450-960 nm spectral range. The best brining salt concentration prediction models developed for raw ($RMSE_p$ 1.9%, $R^2_p$ 0.92) and cooked ($RMSE_p$ 2.6%, $R^2_p$ 0.83) samples used the 957-1664 nm spectral range. This study demonstrates the high potential of hyperspectral imaging as a process analytical tool to classify brined and non-brined pork loins and predict brining salt concentration employed.



## Keywords

Hyperspectral imaging, chemometrics, brining, prediction, classification, pork meat, process analytical technology.

## 1. Introduction

Process analytical technology (PAT) is defined as a system for designing, analysing and controlling manufacturing through timely measurement of critical quality and performance attributes of raw and in process materials and processes, with the goal of ensuring final product quality (FDA, 2004). The adoption of PAT in the food industry is driven by the requirements of regulators, consumers and companies, as well as environmental sustainability (O'Donnell, 2014).

Brining enhances the flavour, texture and shelf life of meat and is widely employed in meat processing. Salt acts as a water binding ingredient in meat products, and helps to solubilise meat proteins and to enhance water holding capacity (WHC) by altering the myofibril structure of proteins (Ruusunen and Puolanne, 2005). Salting also influences the juiciness of meat and product cooking yield (Inguglia et al., 2017; Xiong, 2005). However excess salting may dehydrate meat samples (Barat et al., 2009). Variability in salt uptake can lead to textural defects and can influence the shelf life of the brined pork (Alvarado and McKee, 2007; Fulladosa et al., 2015). Furthermore, the ability to classify brined and non-brined pork, and to predict the brining salt concentration employed during processing are also important from an industry perspective.

Titration techniques are commonly used for salt content determination in meat products (Sharedeh et al., 2015). However these techniques are time consuming, require sample preparation, use of chemicals as well as trained operators (De Prados et al., 2015). Non-destructive technologies have been investigated to monitor the salting process including x-ray absorptiometry, microwave dielectric spectroscopy (Castro-Giráldez et al., 2010), computed tomography (Vestergaard et al., 2004), magnetic induction (Schivazappa et al., 2017), laser induced breakdown spectroscopy (Dixit et al., 2018) and NIR spectroscopy (Campos et al.,

2017; Collell et al., 2011; Collell et al., 2012; Gaitán-Jurado et al., 2008). Application of any of these techniques has not been reported to date to monitor pork brining processes, to classify brined and non-brined pork or to predict brining salt concentration employed.

Spectroscopic sensors provide mainly chemical information but not the spatial information required for analysis of heterogeneous samples such as meat samples (Millar et al., 1996; Prieto et al., 2006). Hyperspectral imaging (HSI) may be suitable for online assessment of brining processes as it provides both spatial and spectral information of samples by combining imaging and spectroscopic tools. HSI is also non-invasive and does not require sample preparation (Gowen et al., 2007). Hyperspectral images or hypercubes are three-dimensional blocks of data, comprising one spectral (wavelength (λ)) and two spatial dimensions (pixels (X, Y)). Each pixel in a hyperspectral image contains the spectrum of that specific position, representing the light-absorbing and/or scattering properties of the spatial region represented, which can be used to characterise the composition of that particular pixel. Hyperspectral imaging has been investigated as a process analytical tool for food applications including on line process control. (Gowen et al., 2007). HSI was used to study salting kinetics of raw pork samples at a fixed brine concentration of 30% salt (Liu et al., 2013). The potential of Vis-NIR hyperspectral imaging to classify brined and non-brined meat samples or predict the brining salt concentration has not been reported to date.

The most common chemometric analysis tools used to evaluate and extract information from hyperspectral imaging data are: (i) principal component analysis (PCA), (ii) partial least squares (PLS) and (iii) variable selection. Spectral pre-treatments may be employed to correct for the effects of natural variability in the shape and size of samples, light scattering and differences in the effective path length on Vis-NIR spectra, which can cause difficulties in the application of HSI for quality assessment (Esquerre et al., 2012b). PCA is one of the most frequently employed techniques for reducing dimensionality of hyperspectral images and is

commonly used as an exploratory tool in analysis of hyperspectral imaging (Burger and Gowen, 2011). PCA can be applied to any data matrix (properly transformed and scaled) to extract the dominant patterns in the matrix in terms of complementary set of scores and loadings plots; with the goal of finding relationships between objects, to delineate classes, to detect outliers, or for data reduction (Geladi et al., 1989). Partial least squares discriminant analysis (PLS-DA) is one of the most frequent classification methods employed in hyperspectral imaging data for classification of objects belonging to one or more classes. Calibration techniques such as partial least squares regression (PLS-R) are routinely employed in hyperspectral imaging analysis for prediction of unknown concentrations and generation of prediction maps to estimate spatial distribution of components in a sample (Gowen et al., 2014). Variable selection methods have been demonstrated to improve the performance of hyperspectral imaging models and to reduce the processing times required by selecting the most informative wavelengths in reported studies including those for the early detection of bruise damage in mushrooms (Esquerre et al., 2011), viability and vigour in muskmelon seeds (Kandpal et al., 2016), fat and moisture content in ground beef (Zhao et al., 2017), internal damage in cucumbers and whole pickles (Ariana and Lu, 2010) and mixing quality of food powders (Achata et al., 2018).

The objective of this study was to investigate the potential of Vis-NIR hyperspectral imaging combined with chemometrics as a process analytical tool to classify brined and non-brined pork loins and predict the brining salt concentration employed for both raw and cooked samples.

## 2. Materials and methods

### 2.1. Pork samples

Fresh pork loins (PLs) (*Longissimus dorsi)* from 16 animals were obtained from local supermarkets and butchers' shops. PLs were trimmed of external fat and connective tissue and divided into samples of 180 ± 20 g and 25 mm thickness (N = 144). Samples obtained from each PL was randomly assigned to treatments.

## 2.2. Sample preparation

### *2.2.1. Brined and non-brined pork samples*

Three types of PL samples were prepared:

i) 'Brined' - immersion in brining solutions at concentrations of 5%, 10% and 15% salt (w/v), prepared using vacuum dried NaCl (food grade) and distilled water at a meat to brine mass ratio of 1:8,

ii) 'Water immersed' - immersion in distilled water without salt (water immersed samples (WI)) and

iii) 'Control' - samples without immersion in water or brine.

### *2.2.2. Raw and cooked samples*

The control samples and half of the brine and water immersed samples were analysed raw (5 (control + 4 treatments) × 16 PLs = 80 raw samples) and the remaining samples were cooked (4 treatments × 16 PLs = 64 cooked samples) in a boiling water bath to a final core temperature of 75 °C, measured by a VWR traceable total-range thermometer (Visalia, CA, USA) placed in the geometric centre of the meat sample (Boccard et al., 1981) and stored at 4 °C prior to analysis.

## 2.3. Hyperspectral imaging systems

Hyperspectral images of raw and cooked PLs were obtained using two line scanning hyperspectral imaging systems (DV Optics, Padova, Italy), one in the visible-near infrared (Vis-NIR) range of 400-1000 nm with a spectral resolution of 5 nm and the other in the near infrared (NIR) range of 880-1720 nm with a spectral resolution of 7 nm. The Vis-NIR-HSI system consisted of a CCD camera (580×580 pixels; Balser, Ahrensburg, Germany), a spectrograph (Spectral Imaging Ltd., Oulu, Finland), cylindrical light diffuser and moving base**.** The NIR-HSI system consisted of an InGaAs camera (320×240 pixels; Sensors Unlimited, Inc., Princeton, NJ, USA), a spectrograph (Spectral Imaging Ltd., Oulu, Finland), five halogen lamps (3×50 W and 2×20 W), a cylindrical light diffuser, moving base and a computer (Hernández-Hierro et al., 2014).The speed of the moving base was set at 3 mm/s (spatial resolution 0.28×0.28 mm pixel size) and 20 mm/s (spatial resolution 0.3×0.3 mm pixel size) for the Vis-NIR and NIR systems respectively. Calibration of both systems was carried out as follows: 50 scan lines of black reference (Ib) were acquired and averaged by taking a measurement after covering the spectrograph lens with a cap; a white tile with a known reflectance (Rw) was placed on the moving base and used as a "white" reference (Iw) by averaging 50 scan lines and finally the signal from the sample (Is) was converted and stored as reflectance (R) according to Equation 1 (Achata et al., 2015).

$$R=\frac{Is - Ib}{Iw - Ib} R_w \qquad (1)$$

Hyperspectral images of all samples were acquired at room temperature (~20 ºC). Spectra were acquired from both sides of all raw and cooked samples. Acquired 3-D data hypercubes were saved in ENVI formatted files and imported into Matlab (The MathWorks Inc., Natick, MA, USA) for further spectral data pre-processing and data analysis (Fig. 1), using in-house developed functions and scripts.

### 2.4. Spectral data pre-processing

Obtained hypercubes were treated as follows:

- The spectra obtained from both HSI systems were trimmed to spectral ranges of 450-960 nm and 957-1664 nm to remove the noise present at both ends of the spectra.
- Hypercubes were unfolded by rearranging the three-dimensional hypercubes (X, Y, λ) into a two-dimensional matrix (X * Y, λ) to facilitate algorithm development.
- The background was removed using a mask which was created by comparing the mean value of each pixel's spectrum and removing pixels with mean spectrum value < 0.7.
- Dead pixels and spikes were removed by replacing the affected values with the mean values of adjacent bands in the same spectrum. Regions of interest (ROI) were carefully selected from each sample to avoid edge effects detected following analysis of PCA scores maps.
- The mean spectra of both sides of each sample was calculated and used for model development.

**2.5. Data analysis**

Principal component analysis (PCA), partial least squares discriminative analysis (PLS-DA), and partial least squares regression (PLS-R) chemometric methods were carried out in combination with spectral pre-treatments on both reflectance and logarithm transformed (log(1/R)) Vis-NIR and NIR-HSI spectral data. EMCVS was applied to improve the performance of the developed models.

For both PLS-DA and PLS-R model development, raw and cooked spectral data sets were randomly split into calibration sets (n = 53 raw; n = 43 cooked) to construct the models and validation sets (n = 27 raw; n = 21 cooked) to test the models. The following spectral pre-

177 treatments were employed to remove scattering effects or baseline shifts and to improve the
178 models' performance: standard normal variate (SNV), median scaled (MS), Savitzky-Golay 7
179 points, second order polynomial first derivative (FD), Savitzky-Golay 7 points, second order
180 polynomial second derivative (SD), linear detrending, second-order polynomial (LD) and
181 asymmetric least squares (AsLs), and all combinations of any two selected pre-treatments.
182 PLS-DA models were developed to discriminate between brined (5, 10 or 15% (w/v), class =
183 0) and non-brined (control & WI, class = 1) samples using a threshold of 0.5. PLS-R models
184 were developed to predict brining salt concentration (BSC). The number of latent variables
185 (LVs) was selected by analysis of the root mean square error of cross validation ($RMSE_{CV}$)
186 and roughness of the regression vector (Gowen et al., 2011).
187 A variable selection approach was also investigated to improve the performance of the
188 models developed. The ensemble Monte Carlo variable selection method (EMCVS) selects
189 wavelengths with the largest mean normalised regression coefficients, which are estimated
190 from an ensemble of Monte Carlo procedures (Esquerre et al., 2011). The EMCVS method
191 was selected as it outperformed other variable selection methods in most cases in previous
192 studies (Esquerre et al., 2011; Esquerre et al., 2017). This method compares the mean of the
193 standardised regression coefficients ($\overline{C_j}$) for each variable in an ensemble of $K$ ($K$ = 200 in
194 this study) Monte Carlo procedures with a threshold in order to select the most informative
195 wavelengths. Only wavelengths with $\overline{C_j}$ value greater than the threshold were retained. For
196 each Monte Carlo procedure regression coefficients (β) were calculated N times using M
197 randomly selected samples to calculate the normalised regression coefficient ($Cjk$) as in Eq.2.

198 $$Cjk = \frac{\overline{\beta}jk}{S(\beta jk)} \quad (2)$$

199 $$\overline{\beta}jk = \left(\sum_{i=1}^{N} \frac{\beta ijk}{N}\right) \quad (3)$$

200 $$S(\beta jk) = \left(\sum_{i=1}^{N} \frac{\beta ijk - \overline{\beta} jk}{N-1}\right) \quad (4)$$

201 Where $\overline{\beta} jk$ and $S(\beta jk)$ are the mean and standard deviation of the regression coefficient of
202 the *j*th variable ($j = 1,2,3,..,p$) over *N* times (*N* = 200 for this study) of all PLS runs and $\beta ijk$
203 is the regression coefficient for the *j*th variable in the *i*th PLS model (*i* = 1…*N*) for the *k*th
204 Monte Carlo procedure (k = 1 … *K*). EMCVS was applied iteratively until no more variables
205 were removed from the data set (Esquerre et al., 2012a; Esquerre et al., 2017).

206

207 **3. Results and discussion**

208 **3.1. Spectral data**

209 Mean log (1/R) spectra of the ROIs for the 450-960 nm and 957-1664 nm spectral ranges are
210 presented in Fig 2a and 2b. It can be observed that baseline shifts and wavelength-dependent
211 variations obscure trends in the spectra associated with the experimental treatments applied.
212 To reduce scattering effects and baseline shifts, Savitzky-Golay spectral pre-treatment (7
213 points, second order polynomial SD) was applied as shown in Fig. 2a and 2b.

214 The main features observed in the 450-960 nm spectra of raw samples in the spectral region
215 of 545-585 nm can be attributed to myoglobin and oxymyoglobin absorptions (Millar et al.,
216 1996; Rannou and Downey, 1997). Brined samples have higher absorption at 580 nm than
217 non-brined samples, which may be related to the oxidation of myoglobin pigments to
218 oxymyoglobin in the presence of salt (Eskin et al., 2013). This is in accordance with
219 previously reported meat studies where the oxidation of myoglobin caused an increase in
220 absorbance at 545 and 575 nm (Kerry et al., 2003; Rannou and Downey, 1997). Spectra of
221 cooked PLs in this region (450-960 nm) exhibit large peaks at 545, 580 and 650 nm which
222 correspond to myoglobin, oxymyoglobin and metmyoglobin respectively (Millar et al., 1996).

The main features that differentiate brined and non-brined samples observed in the 957-1664 nm spectral range of raw samples are at 1153 and 1398 nm, which correspond to the second overtone of C–H bond stretching and C–H combination bands respectively (Osborne et al., 1993). At these wavelengths brined samples have larger peaks than non-brined samples.

In cooked samples, large differences in second derivative spectra of brined and non-brined samples are observed at 1405 nm which correspond to O-H bonds in free water. When salt is added to water, rearrangement of intermolecular hydrogen bonds occurs, resulting in changes to the shape and position of the water peaks in NIR spectra (Gowen et al., 2015).

### 3.2. Principal component analysis

PCA was carried out as an exploratory analysis to detect clustering and outliers using the mean spectra of the hyperspectral images acquired from all raw and cooked samples. Score maps of all samples in the 450-960 nm and 957-1664 nm spectral ranges were visually assessed. The first principal component of both raw and cooked samples explained > 89% of the variance in the spectra, which may be related to experimental treatments applied (Fig. 3). PC1 score maps show a general trend with respect to experimental treatments applied to raw samples. WI and control samples have similar scores and a clear trend was observed with respect to the brining salt concentration. PC1 score maps of cooked samples also show a trend with respect to experimental treatments applied. No clear trends were observed for PC2 score maps of either raw or cooked samples.

Scores and loadings plots for PCA models developed using mean spectra of raw and cooked samples are presented in Fig. 4. Plots of PC1, PC2 and PC3 scores show a general trend with respect to experimental treatments applied to both raw and cooked samples. PC1 and PC2 explained > 97% of the variance in the mean spectra. The PC1 loadings plot for raw samples

247 in the 450-960 nm spectral range show peaks at around 475, 540, 580, 640 and 725 nm which
248 may be related to oxidised/denatured derivatives of myoglobin, myoglobin, oxymyoglobin,
249 metmyoglobin and the 3rd overtone of O-H bond stretching in $H_2O$ respectively (Liu et al.,
250 2000; Millar et al., 1996). The corresponding PC2 loadings plot shows peaks at 555, 585, 640
251 and 725 nm.

252 PC1 loadings plot in the 957-1664 nm spectral range for raw samples shows peaks at around
253 978 nm which correspond to 2nd overtone of O-H bond stretching and may also have
254 contribution from the pigment heme groups in deoxymyoglobin and oxymyoglobin (Liu et
255 al., 2000), at 1181 and 1230 nm due to 2nd overtone of C-H bond stretching in -CH-, -$CH_2$-
256 and -$CH_3$ groups (Shenk et al., 2001; Siesler et al., 2002), and at 1314 nm by combinations of
257 C-H bond stretching in -$CH_3$ groups (Shenk et al., 2001).

258 PC1 and PC2 loadings plots in the 450-960 nm spectral range for cooked samples show peaks
259 at around 540 and 640 nm, related to the effect of salt on the myoglobin and metmyoglobin
260 pigments of the brined samples (Eskin et al., 2013). PC1 loadings plot in the 957-1664 nm
261 spectral range for cooked samples show peaks at around 985, 1188 and 1391 nm
262 (combinations of C-H bonds) related to water protein interaction (Prieto et al., 2006). PC2
263 loadings plot shows peaks at 992, 1146, 1279 and 1461nm (first overtone symmetric N-H
264 bond stretching (Shenk et al., 2001).

265 PCA scores show trends with respect to the BSC employed, which are influenced mainly by
266 heme pigments and water absorption. These results are in general agreement with those
267 reported by Perisic et al. (2013) with a Vis-NIR system in the spectral region of 400-2500
268 nm. These authors found differences in the PCA scores of bovine meat samples due to
269 different salt concentrations.

270

### 3.3. Discrimination of brined and non-brined samples

To discriminate brined (5, 10 and 15% (w/v)) and non-brined (control, WI) samples, a classification approach using PLS-DA was evaluated by assigning arbitrary values to each class (0 for brined and 1 for non-brined samples). The performance of the best PLS-DA models developed to discriminate between brined and non-brined samples are presented in Table 1. Sensitivity (Sen) is the proportion of true positives (class 1 samples) that are correctly identified, while specificity (Spec) is the proportion of true negatives (class 0 samples) that are correctly identified by the model. The geometric mean of sensitivity and specificity ($G = (Sen^2 \times Spec^2)^{0.5}/100$) provides information of the performance of the model in all classes while not being affected by the prevalence of each class in the dataset (Esquerre et al., 2012b; Kubat et al., 1998).

All the developed models for raw samples presented in Table 1 have high discriminant ability as evidenced by G values $\geq 0.91$ in calibration, $G \geq 0.89$ in cross validation and $G \geq 0.95$ in prediction. The best overall model developed for classification of raw samples demonstrated high classification performance (Sen = 100%, Spec = 90%, G = 0.95) for cross-validation and perfect classification for prediction (Sen = 100%, Spec = 100%, G = 1.00) datasets, and was developed using the EMCVS method which selected 18 wavelengths (5 LVs) using SD pre-treated reflectance data in the 957-1664 nm spectral range (Fig. 5). The 18 selected wavelengths used to develop the discriminant model for raw samples are distributed over the 957-1664 nm spectral range and are shown in Fig. 5.

All developed models selected for classification of cooked samples in the 450-960 nm spectral range achieved perfect classification (Sen = 100%, Spec = 100%, G = 1.00). G values $\geq 0.97$ for calibration, cross-validation and prediction datasets were achieved for cooked samples using the 957-1664 nm spectral range. The best overall model (lowest number of variables and LVs) was developed using the EMCVS method which selected 5

296 wavelengths (3 LVs) on the mean log (1/R) data without pre-treatments. The application of
297 the EMCVS method reduced the number of wavelengths employed and the number of latent
298 variables (LVs) in the models developed. Fig. 5 presents the classification of brined and non-
299 brined samples achieved using the best PLS-DA models for cooked samples and the selected
300 bands in the pre-treated mean spectra which achieved the best classification model
301 performance.
302 PLS-DA results for raw samples using the full 450-960 nm spectral range, show better
303 discrimination between brined and not brined samples when no spectral pre-treatments are
304 applied. Previous studies also found better classification results with raw spectra compared to
305 pre-treated spectra in this wavelength range (Folch-Fortuny et al., 2016). Engel et al. (2013)
306 reported a classification case study where less than 5.5 % of pre-processing strategies
307 produced a more accurate and less complex model compared to a model based on raw
308 spectral data. In the full 957-1664 nm spectral range, better discrimination results were
309 obtained when SNV+SD spectral pre-treatments were applied to reflectance and logarithmic
310 transformed spectra. This indicates that the spectra in this range may be affected by
311 multiplicative effects and curved baselines. Previous studies reported that classification
312 models in this region performed better using pre-treated spectra (Kandpal et al., 2016).
313 Discrimination results for cooked samples at both spectral ranges 450-960 nm and 957-1664
314 nm show good discriminant ability when no spectral pre-treatments were applied.

315 PCA and PLS-DA results obtained in this study indicate that discrimination between brined
316 and non-brined of both raw and cooked PLs, is due to the effect of salt on the absorption of
317 Vis NIR electromagnetic energy by myoglobin, O–H and C–H bonds. These results are in
318 accordance with the results reported by Prieto et al. (2015) who obtained the largest
319 regression coefficients in the discrimination of moisture enhanced from non-moisture
320 enhanced pork at the same absorption bands in a spectral range of 350–2500 nm.

### 3.4. Prediction of brine salt concentration

The performance of the PLS-R models was assessed using the root mean square error (RMSE), the coefficient of determination ($R^2$) and the ratio of standard error of prediction to standard deviation (RPD) for calibration, full cross validation, and prediction sets. The performance of the best PLS-R models developed to predict BSC employed using different spectral pre-treatments is presented in Table 2. The models developed for raw samples had $RMSE_P \leq 3.5\%$; $RPD_P$ values ranging from 1.7 to 3.2 and $R^2_P$ values between 0.75 and 0.92 in all cases; while models developed for cooked samples had $RMSE_P$ values $\leq 3.1\%$; $RPD_P$ values ranging from 1.8 to 2.4 and $R^2_P$ values between 0.75 and 0.83 in all cases. The best PLS-R model for raw samples was developed using 34 selected wavelengths of SNV+LD pre-treated log(1/R) spectra (LV 7, $RMSE_P$ 1.9%, $RPD_P$ 3.2, $R^2_P$ 0.92) in the 957-1664 nm spectral range. Most of the selected wavelengths are in the spectral range from 1293 to 1391 nm, where the 2nd overtone of C-H stretching and the 1st overtone of combination of C-H vibration modes are located (Fig. 6). The best PLS-R model for cooked samples was developed using 9 selected wavelengths of SD+SNV pre-treated R spectra (LV 4, $RMSE_P$ 2.6%, $RPD_P$ 2.4, $R^2_P$ 0.83) in the 957-1664 nm spectral range. The selected wavelengths (Fig. 6) are related to the 2nd overtone of C-H stretching (1160, 1202, 1286 nm), the 1st overtone of combination of C-H (1328, 1370 nm), the O-H 2nd overtone (957 nm) and the O-H 1st overtone (1461 and 1559 nm). There is potential to develop a process analytical technology tool using these selected wavelengths for continuous monitoring of meat brining processes.

Prediction results based on full wavelength and with EMCVS selected bands achieved better results with raw samples compared to cooked samples. Better prediction results were achieved using the 957-1664 nm spectral range for both raw and cooked samples on the

logarithmic transformed spectra. De Prados et al. (2015) developed a prediction model for salt content ($R^2 > 0.771$) in pork meat using ultrasound velocity, however no previous studies have been reported on the use of HSI to predict brining salt concentration in meat.

## 4. Conclusions

The results presented in this study demonstrated the potential of Vis-NIR and NIR hyperspectral imaging combined with chemometrics to (i) discriminate between brined and non-brined pork loins using PCA (unsupervised) and PLS-DA (supervised) and (ii) to predict BSC employed using PLS regression for both raw and cooked samples.

PLS-DA models developed perfectly classified raw and cooked pork samples as brined (5, 10 and 15% BSC) or non-brined (control and WI), while PLS-R models with good prediction performance were developed to predict BSC employed (RPD >2.4). The EMCVS variable selection method applied further improved the performance of the PLS-DA and PLS-R models developed.

This study demonstrates the potentiality of employing Vis-NIR hyperspectral imaging coupled with chemometrics as a rapid and non-destructive process analytical technology to monitor and control pork loins brining processes. Adoption of this PAT tool by meat processors would enhance quality assurance, process control and validation in meat brining processes.

## Acknowledgements

The authors acknowledge funding for this project from FIRM (13/FM/508) as administered by the Irish Department of Agriculture, Food & the Marine.

## References

Achata, E., Esquerre, C., O'Donnell, C., Gowen, A., (2015). A study on the application of near infrared hyperspectral chemical imaging for monitoring moisture content and water activity in low moisture systems. Molecules 20(2), 2611-2621.

Achata, E.M., Esquerre, C., Gowen, A.A., O'Donnell, C.P., (2018). Feasibility of near infrared and raman hyperspectral imaging combined with multivariate analysis to assess binary mixtures of food powders. Powder Technology 336, 555-566.

Alvarado, C., McKee, S., (2007). Marination to improve functional properties and safety of poultry meat. The Journal of Applied Poultry Research 16(1), 113-120.

Ariana, D.P., Lu, R., (2010). Hyperspectral waveband selection for internal defect detection of pickling cucumbers and whole pickles. Computers and Electronics in Agriculture 74(1), 137-144.

Barat, J.M., Aliño, M., Fuentes, A., Grau, R., Romero, J.B., (2009). Measurement of swelling pressure in pork meat brining. Journal of Food Engineering 93(1), 108-113.

Boccard, R., Buchter, L., Casteels, E., Cosentino, E., Dransfield, E., Hood, D.E., Joseph, R.L., MacDougall, D.B., Rhodes, D.N., Schön, I., Tinbergen, B.J., Touraille, C., (1981). Procedures for measuring meat quality characteristics in beef production experiments. Report of a working group in the commission of the european communities' (cec) beef production research programme. Livestock Production Science 8(5), 385-397.

Burger, J., Gowen, A., (2011). Data handling in hyperspectral image analysis. Chemometrics and Intelligent Laboratory Systems 108(1), 13-22.

Campos, M.I., Mussons, M.L., Antolin, G., Debán, L., Pardo, R., (2017). On-line prediction of sodium content in vacuum packed dry-cured ham slices by non-invasive near infrared spectroscopy. Meat Science 126(Supplement C), 29-35.

Castro-Giráldez, M., Fito, P.J., Fito, P., (2010). Application of microwaves dielectric spectroscopy for controlling pork meat (longissimus dorsi) salting process. Journal of Food Engineering 97(4), 484-490.

Collell, C., Gou, P., Arnau, J., Comaposada, J., (2011). Non-destructive estimation of moisture, water activity and nacl at ham surface during resting and drying using nir spectroscopy. Food Chemistry 129(2), 601-607.

Collell, C., Gou, P., Arnau, J., Muñoz, I., Comaposada, J., (2012). Nir technology for on-line determination of superficial aw and moisture content during the drying process of fermented sausages. Food Chemistry 135(3), 1750-1755.

De Prados, M., García-Pérez, J.V., Benedito, J., (2015). Non-destructive salt content prediction in brined pork meat using ultrasound technology. Journal of Food Engineering 154(Supplement C), 39-48.

Dixit, Y., Casado-Gavalda, M.P., Cama-Moncunill, R., Cama-Moncunill, X., Markiewicz-Keszycka, M., Jacoby, F., Cullen, P.J., Sullivan, C., (2018). Introduction to laser induced breakdown spectroscopy imaging in food: Salt diffusion in meat. Journal of Food Engineering 216, 120-124.

409 Engel, J., Gerretzen, J., Szymańska, E., Jansen, J.J., Downey, G., Blanchet, L., Buydens, L.M.C., (2013).
410 Breaking with trends in pre-processing? TRAC Trends in Analytical Chemistry 50, 96-106.
411 Eskin, N.A.M., Aliani, M., Shahidi, F., (2013). Chapter 3 - meat and fish, in: Eskin, N.A.M., Shahidi, F.
412 (Eds.), *Biochemistry of foods (third edition)*. Academic Press, San Diego, pp. 127-185.
413 Esquerre, C., Gowen, A., Downey, G., O'Donnell, C., (2012a). Wavelength selection for development
414 of a near infrared imaging system for early detection of bruise damage in mushrooms
415 (agaricus bisporus). Journal of Near Infrared Spectroscopy 20(5), 537-546.
416 Esquerre, C., Gowen, A.A., Burger, J., Downey, G., O'Donnell, C.P., (2012b). Suppressing sample
417 morphology effects in near infrared spectral imaging using chemometric data pre-
418 treatments. Chemometrics and Intelligent Laboratory Systems 117, 129-137.
419 Esquerre, C., Gowen, A.A., Downey, G., O'Donnell, C.P., (2011). Selection of variables based on most
420 stable normalised partial least squares regression coefficients in an ensemble monte carlo
421 procedure. Journal of Near Infrared Spectroscopy 19(6), 443-450.
422 Esquerre, C.A., Gowen, A.A., O'Gorman, A., Downey, G., O'Donnell, C.P., (2017). Evaluation of
423 ensemble monte carlo variable selection for identification of metabolite markers on nmr
424 data. Analytica Chimica Acta 964, 45-54.
425 FDA, (2004). Guidance for industry pat - a framework for innnovative pharmaceutical development,
426 manufacturing and quality assurance.
427 Folch-Fortuny, A., Prats-Montalbán, J.M., Cubero, S., Blasco, J., Ferrer, A., (2016). Vis/nir
428 hyperspectral imaging and n-way pls-da models for detection of decay lesions in citrus fruits.
429 Chemometrics and Intelligent Laboratory Systems 156, 241-248.
430 Fulladosa, E., Muñoz, I., Serra, X., Arnau, J., Gou, P., (2015). X-ray absorptiometry for non-destructive
431 monitoring of the salt uptake in bone-in raw hams during salting. Food Control 47, 37-42.
432 Gaitán-Jurado, A.J., Ortiz-Somovilla, V., España-España, F., Pérez-Aparicio, J., De Pedro-Sanz, E.J.,
433 (2008). Quantitative analysis of pork dry-cured sausages to quality control by nir
434 spectroscopy. Meat Science 78(4), 391-399.
435 Geladi, P., Isaksson, H., Lindqvist, L., Wold, S., Esbensen, K., (1989). Principal component analysis of
436 multivariate images. Chemometrics and Intelligent Laboratory Systems 5(3), 209-220.
437 Gowen, A., Burger, J., Esquerre, C., Downey, G., O'Donnell, C., (2014). Near infrared hyperspectral
438 image regression: On the use of prediction maps as a tool for detecting model overfitting.
439 Journal of Near Infrared Spectroscopy 22(4), 261-270.
440 Gowen, A.A., Downey, G., Esquerre, C., O'Donnell, C.P., (2011). Preventing over-fitting in pls
441 calibration models of near-infrared (nir) spectroscopy data using regression coefficients.
442 Journal of Chemometrics 25(7), 375-381.
443 Gowen, A.A., Marini, F., Tsuchisaka, Y., De Luca, S., Bevilacqua, M., O'Donnell, C., Downey, G.,
444 Tsenkova, R., (2015). On the feasibility of near infrared spectroscopy to detect contaminants
445 in water using single salt solutions as model systems. Talanta 131(Supplement C), 609-618.
446 Gowen, A.A., O'Donnell, C.P., Cullen, P.J., Downey, G., Frias, J.M., (2007). Hyperspectral imaging – an
447 emerging process analytical tool for food quality and safety control. Trends in Food Science
448 & Technology 18(12), 590-598.
449 Hernández-Hierro, J.M., Esquerre, C., Valverde, J., Villacreces, S., Reilly, K., Gaffney, M., González-
450 Miret, M.L., Heredia, F.J., O'Donnell, C.P., Downey, G., (2014). Preliminary study on the use
451 of near infrared hyperspectral imaging for quantitation and localisation of total
452 glucosinolates in freeze-dried broccoli. Journal of Food Engineering 126, 107-112.
453 Inguglia, E.S., Zhang, Z., Tiwari, B.K., Kerry, J.P., Burgess, C.M., (2017). Salt reduction strategies in
454 processed meat products – a review. Trends in Food Science & Technology 59(Supplement
455 C), 70-78.
456 Kandpal, L.M., Lohumi, S., Kim, M.S., Kang, J.-S., Cho, B.-K., (2016). Near-infrared hyperspectral
457 imaging system coupled with multivariate methods to predict viability and vigor in
458 muskmelon seeds. Sensors and Actuators B: Chemical 229, 534-544.

459 Kerry, J., Kerry, J., Ledward, D., (2003). Meat processing improving quality. CRC Press, Boca Raton,
460 Fla; Cambridge, England.
461 Kubat, M., Holte, R.C., Matwin, S., (1998). Machine learning for the detection of oil spills in satellite
462 radar images. Machine Learning 30(2), 195-215.
463 Liu, D., Qu, J., Sun, D.-W., Pu, H., Zeng, X.-A., (2013). Non-destructive prediction of salt contents and
464 water activity of porcine meat slices by hyperspectral imaging in a salting process. Innovative
465 Food Science & Emerging Technologies 20(Supplement C), 316-323.
466 Liu, Y., Chen, Y.-R., Ozaki, Y., (2000). Two-dimensional visible/near-infrared correlation spectroscopy
467 study of thermal treatment of chicken meats. Journal of Agricultural and Food Chemistry
468 48(3), 901-908.
469 Millar, S.J., Moss, B.W., Stevenson, M.H., (1996). Some observations on the absorption spectra of
470 various myoglobin derivatives found in meat. Meat Science 42(3), 277-288.
471 O'Donnell, C.P., Fagan, Colette, Cullen, P.J. (Eds.), (2014). Process analytical technology for the food
472 industry. Springer-Verlag New York.
473 Osborne, B., Fearn, T., Hindle, P.H., (1993). *Practical nir spectroscopy with applications in food and*
474 *beverage analysis* (Second ed). Longman, Singapore.
475 Perisic, N., Afseth, N.K., Ofstad, R., Hassani, S., Kohler, A., (2013). Characterising protein, salt and
476 water interactions with combined vibrational spectroscopic techniques. Food Chemistry
477 138(1), 679-686.
478 Prieto, N., Andrés, S., Giráldez, F.J., Mantecón, A.R., Lavín, P., (2006). Potential use of near infrared
479 reflectance spectroscopy (nirs) for the estimation of chemical composition of oxen meat
480 samples. Meat Science 74(3), 487-496.
481 Prieto, N., Juárez, M., Larsen, I.L., López-Campos, Ó., Zijlstra, R.T., Aalhus, J.L., (2015). Rapid
482 discrimination of enhanced quality pork by visible and near infrared spectroscopy. Meat
483 Science 110, 76-84.
484 Rannou, H., Downey, G., (1997). Discrimination of raw pork, chicken and turkey meat by
485 spectroscopy in the visible, near- and mid-infrared ranges. Analytical Communications
486 34(12), 401-404.
487 Ruusunen, M., Puolanne, E., (2005). Reducing sodium intake from meat products. Meat Science
488 70(3), 531-541.
489 Schivazappa, C., Virgili, R., Simoncini, N., Tiso, S., Álvarez, J., Rodríguez, J.M., (2017). Application of
490 the magnetic induction technique for the non-destructive assessment of salt gain after the
491 salting process of parma ham. Food Control 80(Supplement C), 92-98.
492 Sharedeh, D., Mirade, P.-S., Venien, A., Daudin, J.-D., (2015). Analysis of salt penetration
493 enhancement in meat tissue by mechanical treatment using a tumbling simulator. Journal of
494 Food Engineering 166(Supplement C), 377-383.
495 Shenk, J.S., Workman, J.J., Westerhaus, M.O., (2001). Chapter 17: Application of nir spectroscopy to
496 agricultural products, in: Burns, D.A., Ciurczak, E.W. (Eds.), *Handbook of near infrared*
497 *analysis*, Third ed. CRC Press, New York, pp. 347-386.
498 Siesler, H.W., Ozaki, Y., Kawata, S., Heise, H.M., (2002). Near-infrared spectroscopy: Principles,
499 instruments, applications. Wiley, Weinheim, p. 348.
500 Vestergaard, C., Risum, J., Adler-Nissen, J., (2004). Quantification of salt concentrations in cured pork
501 by computed tomography. Meat Science 68(1), 107-113.
502 Xiong, Y.L., (2005). Role of myofibrillar proteins in water-binding in brine-enhanced meats. Food
503 Research International 38(3), 281-287.
504 Zhao, M., Esquerre, C., Downey, G., O'Donnell, C.P., (2017). Process analytical technologies for fat
505 and moisture determination in ground beef - a comparison of guided microwave
506 spectroscopy and near infrared hyperspectral imaging. Food Control 73, 1082-1094.

**Table 1:** Performance of the PLS-DA models developed for discrimination of brined and non-brined samples

| | Pre-treatment | EMCVS | # Bands | # LVs | Calibration | | | Cross validation | | | Prediction | | |
|---|---|---|---|---|---|---|---|---|---|---|---|---|---|
| | | | | | $Sen_C$ (%) | $Spec_C$ (%) | $G_C$ | $Sen_{CV}$ (%) | $Spec_{CV}$ (%) | $G_{CV}$ | $Sen_P$ (%) | $Spec_P$ (%) | $G_p$ |
| **Raw 450-960 nm** | | | | | | | | | | | | | |
| R | None | No | 103 | 6 | 96 | 97 | 0.96 | 92 | 93 | 0.92 | 100 | 95 | 0.97 |
| | AsLs+LD | Yes | 19 | 5 | 100 | 97 | 0.98 | 100 | 97 | 0.98 | 100 | 89 | 0.95 |
| log(1/R) | None | No | 103 | 9 | 96 | 97 | 0.96 | 96 | 93 | 0.94 | 100 | 89 | 0.95 |
| | LD | Yes | 10 | 6 | 100 | 97 | 0.98 | 100 | 97 | 0.98 | 100 | 89 | 0.95 |
| **Raw 957-1664 nm** | | | | | | | | | | | | | |
| R | SNV+SD | No | 96 | 4 | 100 | 83 | 0.91 | 100 | 79 | 0.89 | 100 | 95 | 0.97 |
| | **SD** | **Yes** | **18** | **5** | **100** | **93** | **0.96** | **100** | **90** | **0.95** | **100** | **100** | **1.00** |
| log(1/R) | SNV+SD | No | 96 | 5 | 100 | 97 | 0.98 | 96 | 90 | 0.93 | 100 | 95 | 0.97 |
| | AsLs+MS | Yes | 13 | 6 | 88 | 97 | 0.92 | 88 | 97 | 0.92 | 100 | 100 | 1.00 |
| **Cooked 450-960 nm** | | | | | | | | | | | | | |
| R | None | No | 103 | 4 | 100 | 100 | 1.00 | 100 | 100 | 1.00 | 100 | 100 | 1.00 |
| | None | Yes | 8 | 4 | 100 | 100 | 1.00 | 100 | 100 | 1.00 | 100 | 100 | 1.00 |
| log(1/R) | None | No | 103 | 3 | 100 | 100 | 1.00 | 100 | 100 | 1.00 | 100 | 100 | 1.00 |
| | **None** | **Yes** | **5** | **3** | **100** | **100** | **1.00** | **100** | **100** | **1.00** | **100** | **100** | **1.00** |
| **Cooked 957-1664 nm** | | | | | | | | | | | | | |
| R | None | No | 102 | 2 | 100 | 100 | 1.00 | 100 | 100 | 1.00 | 100 | 93 | 0.97 |
| | None | Yes | 4 | 1 | 100 | 100 | 1.00 | 100 | 100 | 1.00 | 100 | 93 | 0.97 |
| log(1/R) | None | No | 102 | 1 | 100 | 100 | 1.00 | 100 | 100 | 1.00 | 100 | 93 | 0.97 |
| | None | Yes | 1 | 1 | 100 | 100 | 1.00 | 100 | 100 | 1.00 | 100 | 93 | 0.97 |

EMCVS, ensemble Monte Carlo variable selection; LD, linear detrending; FD, first derivative; MS, median scaled; SD, second derivative; SNV, standard normal variate; AsLs, asymmetric least squares; Bands, wavelengths used for model development; LVs, latent variables; $Sen_{CV}$, sensitivity for cross-validation; $Spec_{CV}$ specificity for cross-validation; $Sen_P$, sensitivity for prediction; $Spec_P$ specificity for prediction.
The overall best models for raw and cooked samples are highlighted in bold.

514 **Table 2:** Performance of the PLS-R models developed for the prediction of brine salt concentration (BSC) in brined pork.

| | Pre-treatment | EMCVS | # Bands | # LVs | Calibration | | | Cross validation | | | Prediction | | |
|---|---|---|---|---|---|---|---|---|---|---|---|---|---|
| | | | | | $RMSE_C$ | $RPD_C$ | $R_c^2$ | $RMSE_{CV}$ | $RPD_{CV}$ | $Rcv^2$ | $RMSE_p$ | $RPD_p$ | $R_P^2$ |
| **Raw 450-960 nm** | | | | | | | | | | | | | |
| R | FD+SNV | No | 97 | 7 | 2.7 | 2.2 | 0.79 | 3.7 | 1.6 | 0.60 | 2.6 | 2.2 | 0.84 |
| | SD | Yes | 18 | 8 | 2.2 | 2.6 | 0.86 | 2.3 | 2.5 | 0.84 | 3.5 | 1.7 | 0.76 |
| log(1/R) | LD+FD | No | 97 | 6 | 2.7 | 2.2 | 0.79 | 3.6 | 1.6 | 0.61 | 2.6 | 2.1 | 0.82 |
| | FD | Yes | 7 | 4 | 2.5 | 2.3 | 0.82 | 3.0 | 1.9 | 0.72 | 2.6 | 2.3 | 0.82 |
| **Raw 957-1664 nm** | | | | | | | | | | | | | |
| R | AsLs+SNV | No | 102 | 7 | 1.7 | 3.3 | 0.91 | 2.3 | 2.5 | 0.84 | 2.1 | 2.7 | 0.90 |
| | SNV+FD | Yes | 9 | 3 | 2.4 | 2.4 | 0.83 | 2.3 | 2.5 | 0.84 | 2.2 | 2.8 | 0.88 |
| log(1/R) | MS+SNV | No | 102 | 8 | 1.5 | 3.7 | 0.93 | 2.5 | 2.3 | 0.81 | 1.9 | 3.0 | 0.94 |
| | **SNV+LD** | **Yes** | **34** | **7** | **1.5** | **3.7** | **0.93** | **2.1** | **2.8** | **0.87** | **1.9** | **3.2** | **0.92** |
| **Cooked 450-960 nm** | | | | | | | | | | | | | |
| R | SNV+LD | No | 103 | 9 | 2.2 | 2.5 | 0.84 | 2.1 | 2.6 | 0.85 | 2.9 | 1.8 | 0.75 |
| | LD | Yes | 14 | 6 | 2.2 | 2.5 | 0.84 | 1.9 | 2.9 | 0.88 | 3.0 | 2.0 | 0.75 |
| log(1/R) | AsLs+SNV | No | 103 | 10 | 2.3 | 2.4 | 0.83 | 2.3 | 2.4 | 0.83 | 3.1 | 1.8 | 0.75 |
| | SNV+SD | Yes | 21 | 6 | 2.3 | 2.4 | 0.83 | 2.0 | 2.8 | 0.87 | 3.0 | 2.0 | 0.74 |
| **Cooked 957-1664 nm** | | | | | | | | | | | | | |
| R | SD+AsLs | No | 96 | 6 | 1.9 | 2.9 | 0.88 | 2.5 | 2.2 | 0.79 | 2.8 | 2.1 | 0.79 |
| | **SD+SNV** | **Yes** | **9** | **4** | **2.0** | **2.8** | **0.87** | **2.0** | **2.7** | **0.86** | **2.6** | **2.4** | **0.83** |
| log(1/R) | MS+FD | No | 96 | 7 | 1.8 | 3.0 | 0.89 | 1.9 | 2.9 | 0.88 | 2.7 | 2.0 | 0.79 |
| | MS+FD | Yes | 17 | 6 | 1.8 | 3.1 | 0.89 | 1.6 | 3.4 | 0.91 | 2.6 | 2.3 | 0.81 |

515 EMCVS, ensemble Monte Carlo variable selection; FD, first derivative; LD, linear detrending; SD, second derivative; SNV, Standard normal
516 variate; AsLs, asymmetric least squares; MS, median scaled; Bands, wavelengths used for model development; LVs, latent variables.
517 The overall best models for raw and cooked samples are highlighted in bold.

Figure captions

Fig. 1. Hyperspectral imaging and data analysis.

Fig. 2. Mean log(1/R) and second derivative of mean log(1/R) spectra of (a) raw and (b) cooked samples.

Fig. 3. PCA score maps of log(1/R) spectra of (a) raw and (b) cooked samples.

Fig. 4. PCA score plots and loadings of mean log(1/R) spectra of (a) raw and (b) cooked samples.

Fig. 5. Classification of brined and non-brined samples using the best PLS-DA models developed for (a) raw (SD on the reflectance spectra 957–1664 nm), and (b) cooked samples (log (1/R) spectra without spectral pre-treatment 450–960 nm).

Fig. 6. Brining salt concentration predicted using the best PLS-R models developed for (a) raw (SNV+LD spectral pre-treatments on the log (1/R) spectra 957–1664 nm), and (b) cooked samples (SD+SNV spectral pre-treatments on the reflectance spectra 957–1664 nm).

**Highlights**

- Vis-NIR hyperspectral imaging is suitable for the assessment of brining of raw and cooked pork loins.
- Chemometric models were developed to classify brined and non-brined pork samples and to predict brining salt concentration employed.
- Spectral pre-treatments and variable selection improved performance of models developed.

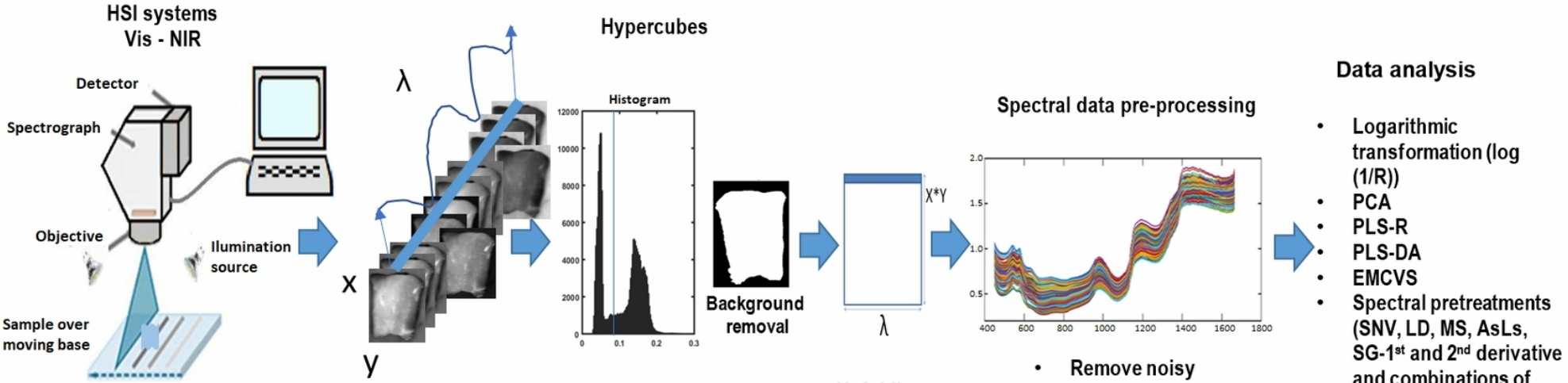
HSI systems
Vis - NIR
Detector
Spectrograph
Objective
Ilumination source
Sample over moving base
λ
x
y
Hypercubes
Histogram
Thresholding
Background removal
Unfolding
x*y
λ
Spectral data pre-processing
Data analysis
Logarithmic transformation (log (1/R))
PCA
PLS-R
PLS-DA
EMCVS
Spectral pretreatments (SNV, LD, MS, AsLs, SG-1st and 2nd derivative and combinations of any two of them)
Line scanning from 400 to 1720 nm.
Raw and cooked samples scanned
Data recorded as reflectance in ENVI format.
Remove noisy bands by trimming spectra
Eliminate dead pixels

(a) Raw

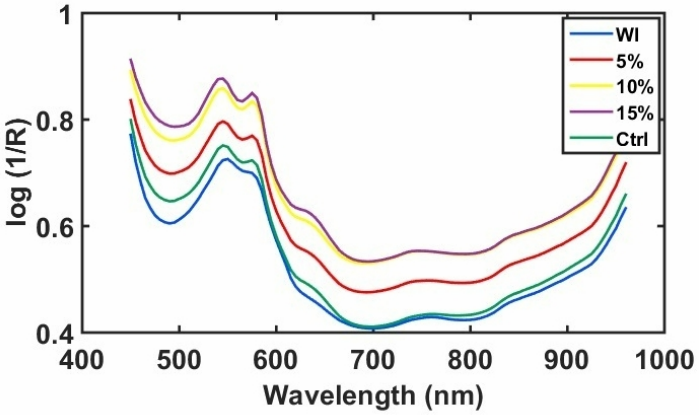


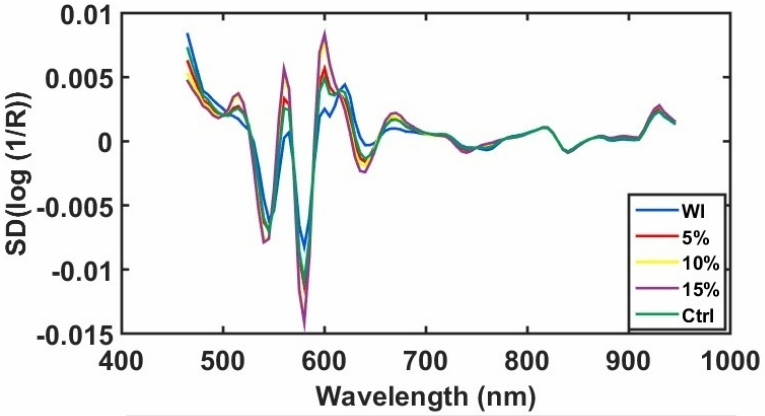


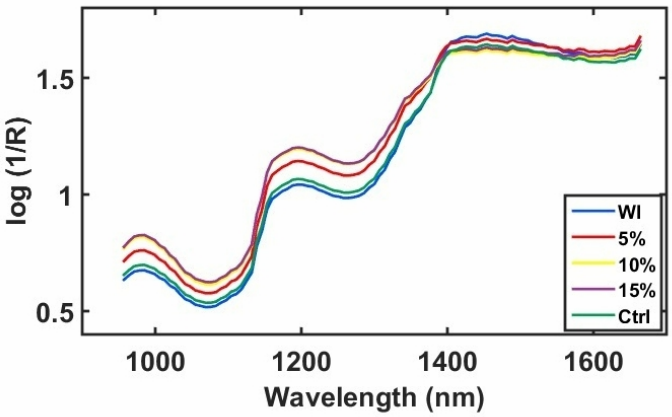


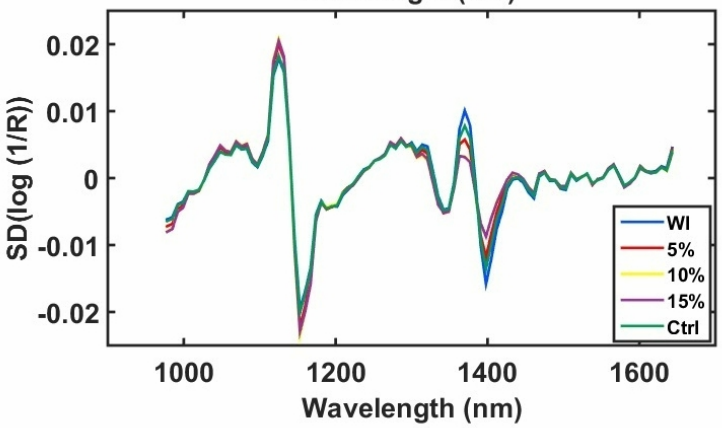


(b) Cooked

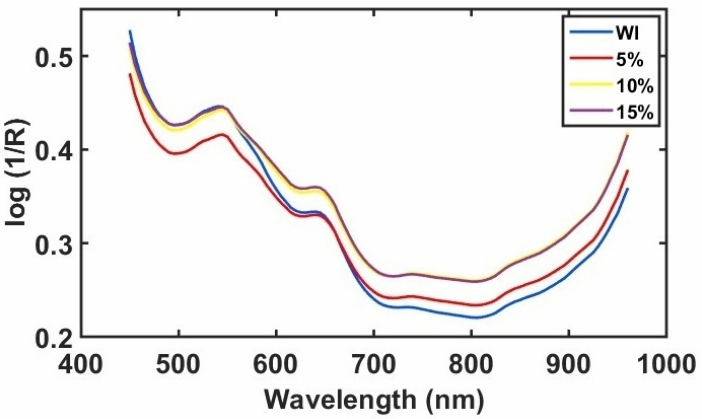


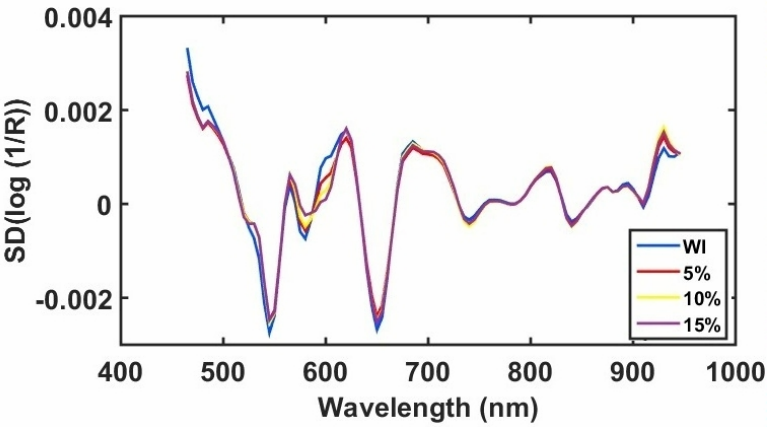


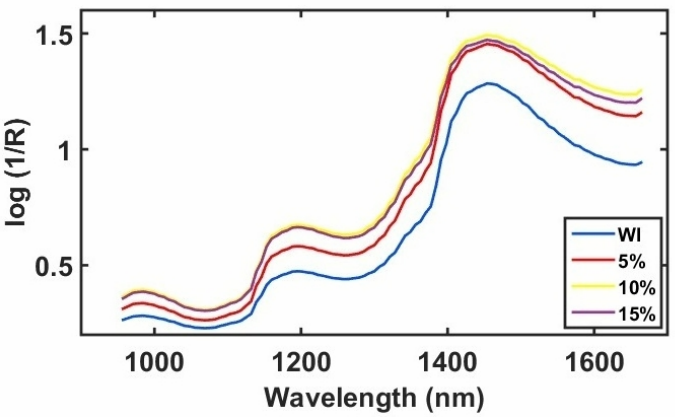


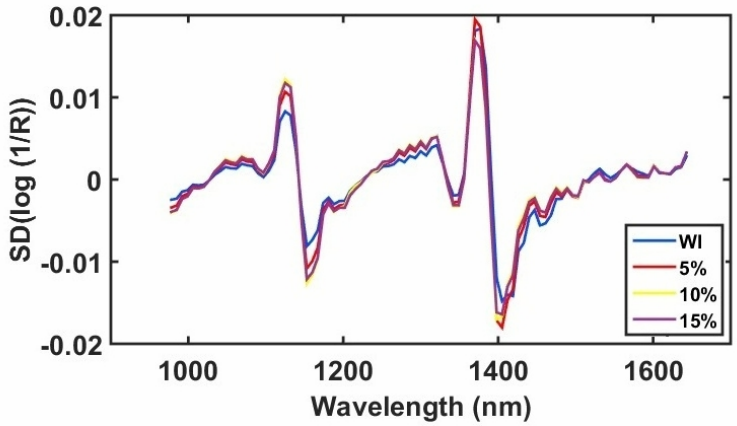

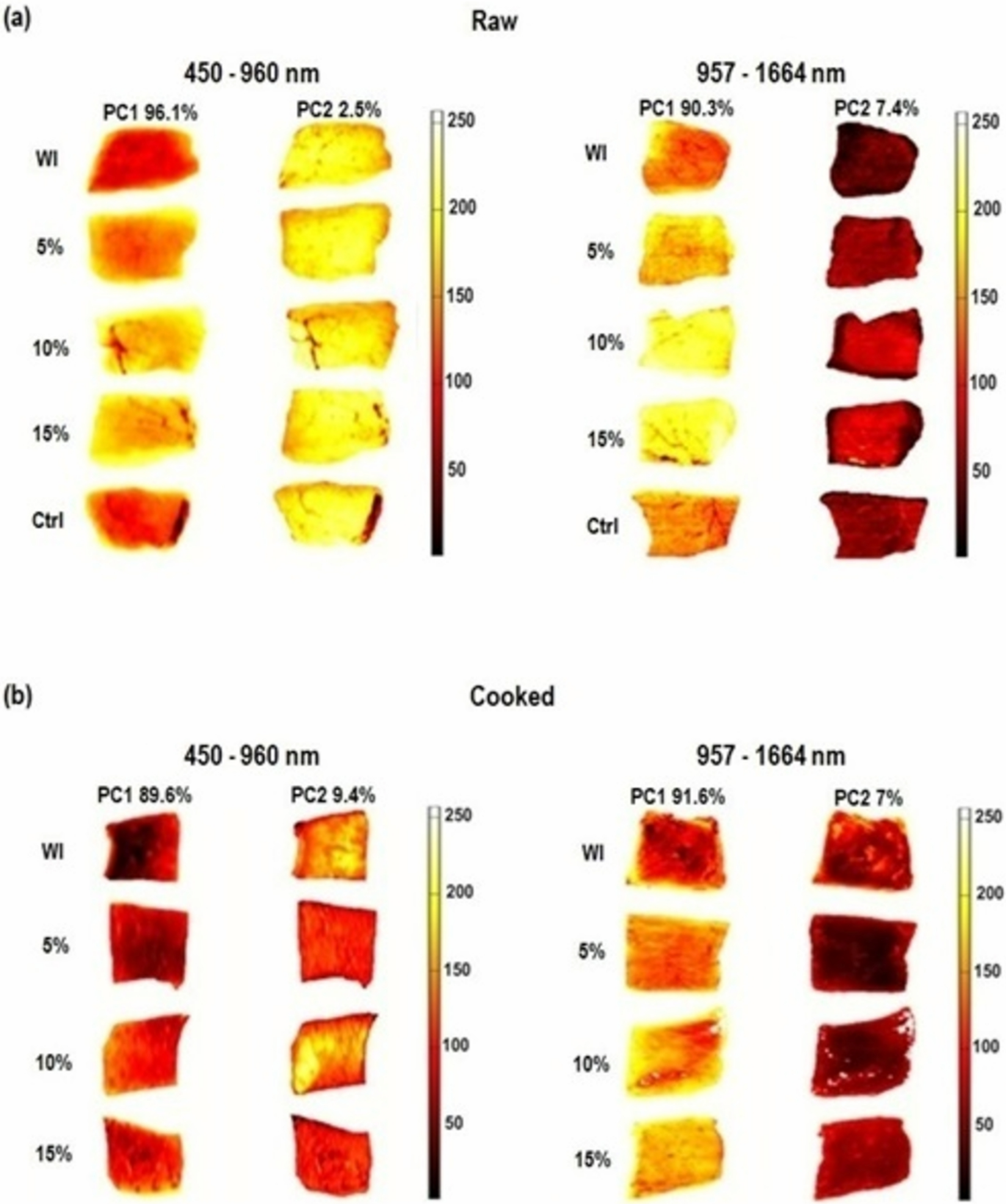
(a)
Raw
450 - 960 nm
957 - 1664 nm
PC1 96.1%
PC2 2.5%
PC1 90.3%
PC2 7.4%
WI
5%
10%
15%
Ctrl
250
200
150
100
50
(b)
Cooked
450 - 960 nm
957 - 1664 nm
PC1 89.6%
PC2 9.4%
PC1 91.6%
PC2 7%
WI
5%
10%
15%
250
200
150
100
50

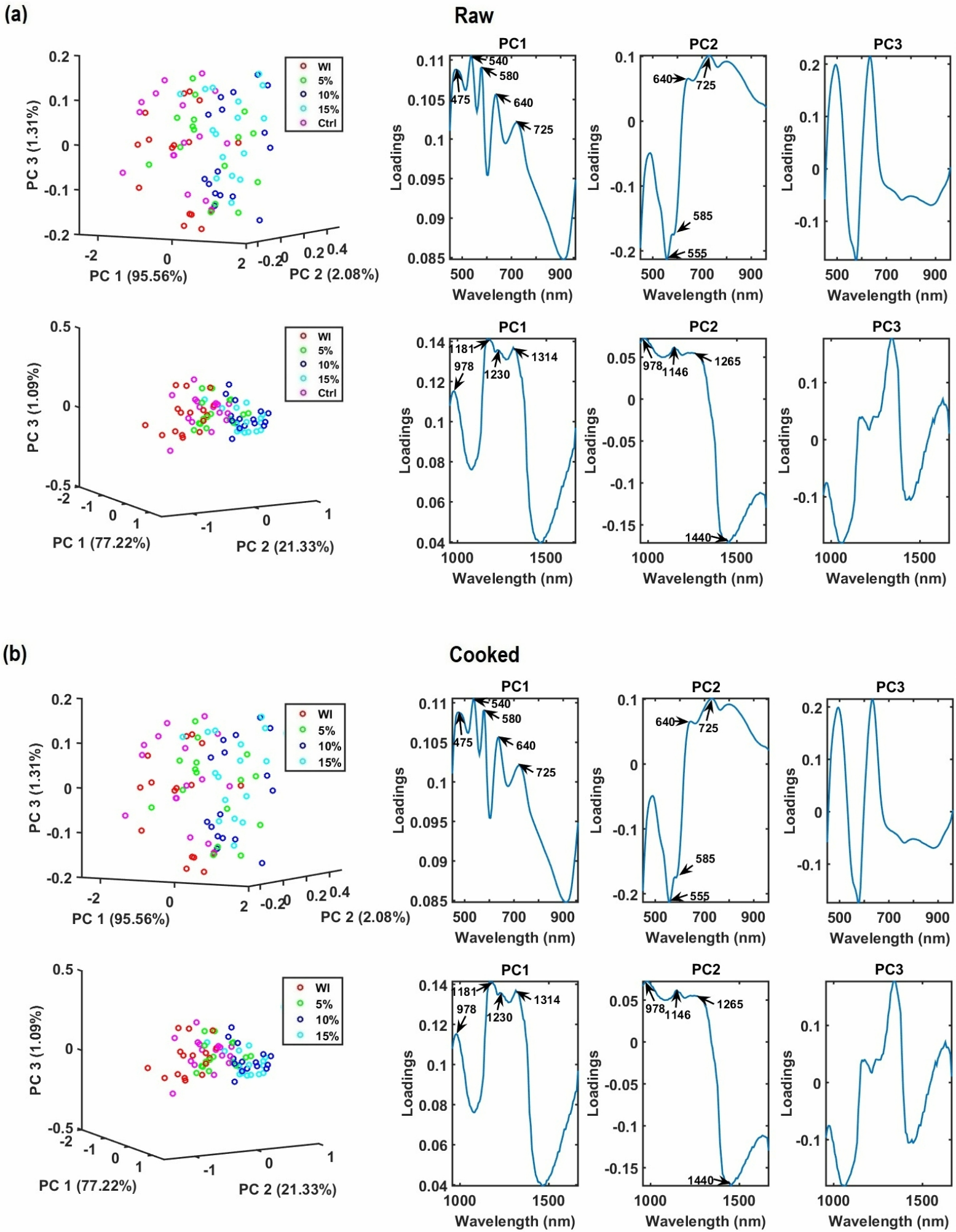
(a)
Raw
WI
5%
10%
15%
Ctrl
PC 1 (95.56%)
PC 2 (2.08%)
PC 3 (1.31%)
PC 1 (77.22%)
PC 2 (21.33%)
PC 3 (1.09%)
PC1
PC2
PC3
Loadings
Wavelength (nm)
540
580
475
640
725
585
555
1181
978
1230
1314
1146
1265
1440
(b)
Cooked

(a)

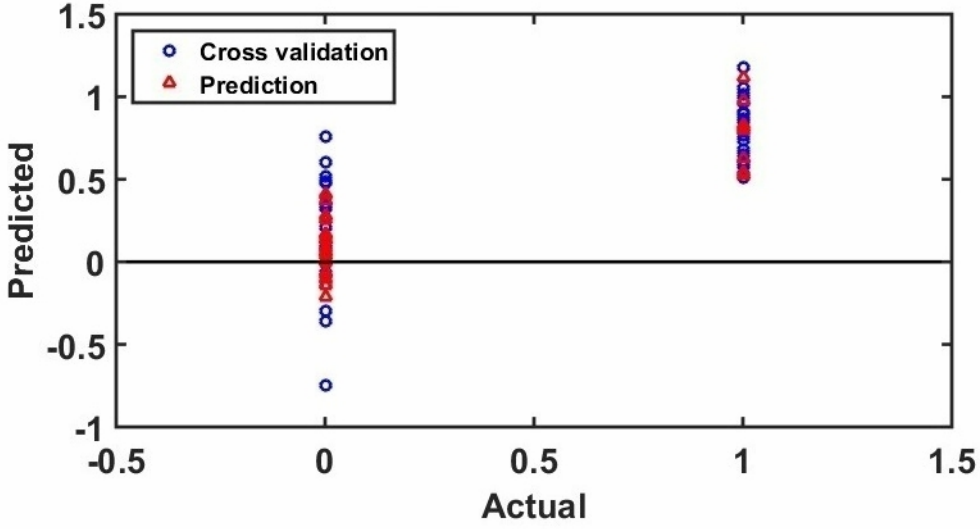


Raw

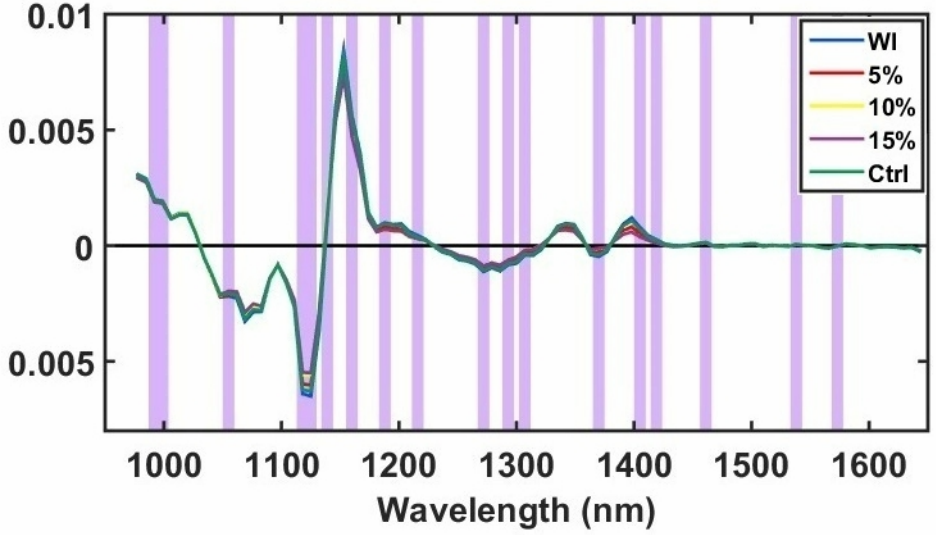


(b)

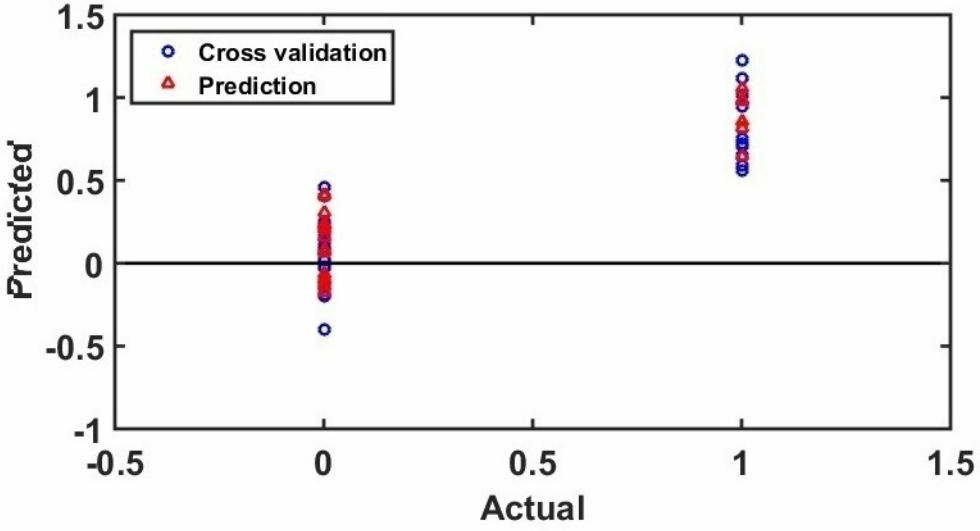


Cooked

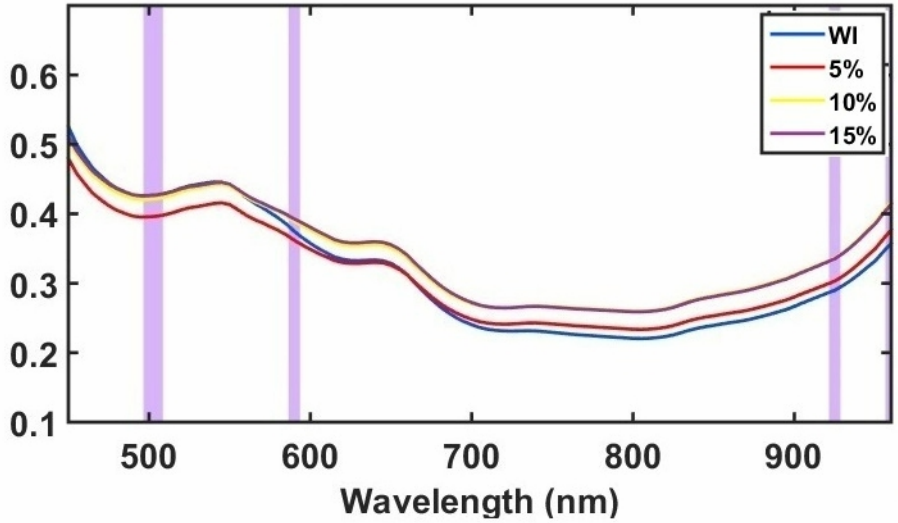

(a)

Raw

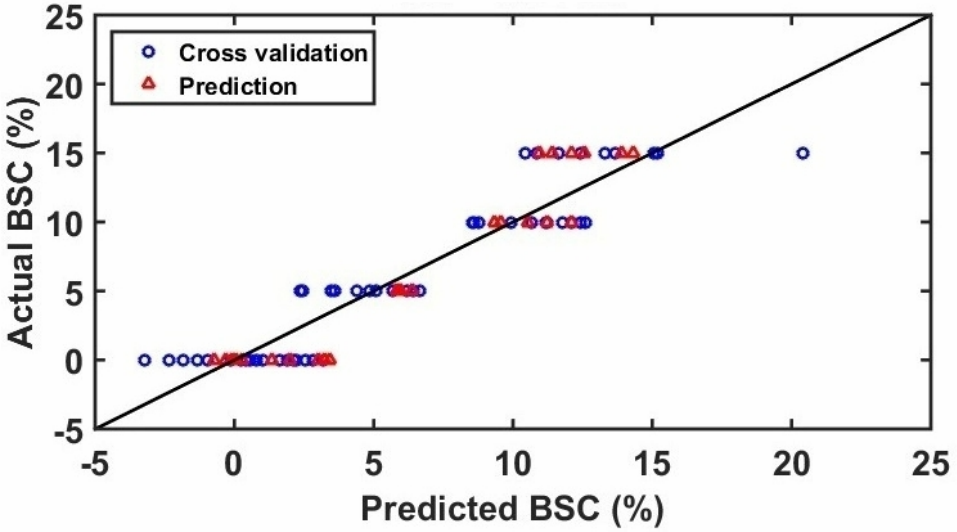


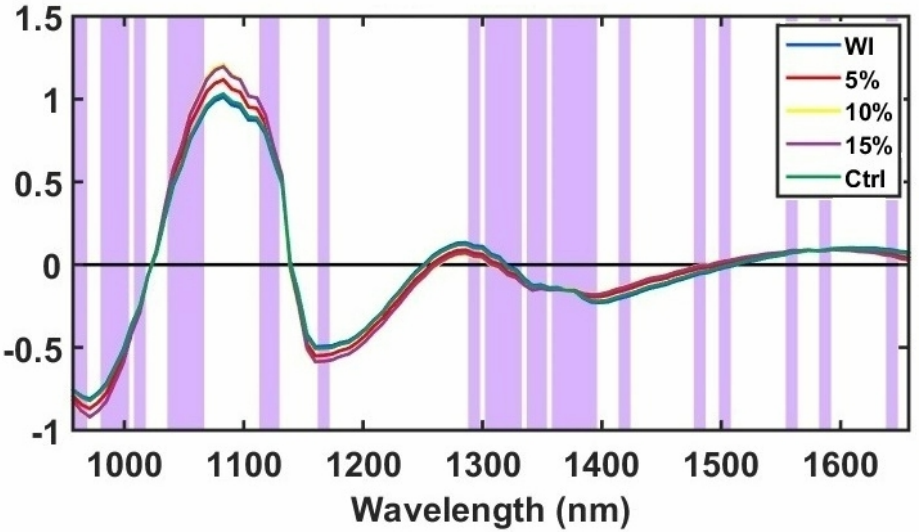


(b)

Cooked